Vacuum-ultraviolet photodissociation of C2H2 via Rydberg states: A study of the fluorescent pathways

ARTICLE *in* CHEMICAL PHYSICS LETTERS · NOVEMBER 1999

Impact Factor: 1.9 · DOI: 10.1016/S0009-2614(99)01121-5

7 AUTHORS, INCLUDING:

Stéphane Douin
Université Paris-Sud 11
41 PUBLICATIONS **390** CITATIONS
SEE PROFILE

C. E. Fellows
Universidade Federal Fluminense
67 PUBLICATIONS **676** CITATIONS
SEE PROFILE

26 November 1999

ELSEVIER

Chemical Physics Letters 314 (1999) 91–100

CHEMICAL PHYSICS LETTERS

www.elsevier.nl/locate/cplett

Vacuum–ultraviolet photodissociation of C_2H_2 via Rydberg states: a study of the fluorescent pathways

A. Campos [a,b,c], S. Boyé [a], Ph. Bréchignac [a], S. Douin [a], C. Fellows [a,b,c], N. Shafizadeh [a], D. Gauyacq [a,*]

[a] *Laboratoire de Photophysique Moléculaire, Bât. 210, Campus d'Orsay, Orsay 91405, France*
[b] *Bolsista CAPES, Brasília, Brazil*
[c] *Instituto de Física, Universidade Federal Fuminense, Niterói, RJ, Brazil*

Received 30 July 1999; in final form 10 September 1999

Abstract

The visible fluorescence produced by vacuum–ultraviolet photodissociation of acetylene, particularly through the Rydberg states, has been studied in a gas-flow system using synchrotron radiation as a light source between 154 and 60 nm and an original light collection device. Excitation of the Rydberg states below the first IP reveals only the C_2H product by its $\tilde{A}$–$\tilde{X}$ continuum emission spectrum between 330 and 900 nm. Evolution in the emission spectral profile as a function of excitation wavelength has been observed, indicative of specific internal distribution favoring the bending levels of the $\tilde{A}$ state of C_2H. A new assignment of the Rydberg series converging to the first excited state $\tilde{A}\,^2A_g$ of the cation is proposed on the basis of recent experimental and theoretical characterization of this state and leads to an approximate value of the C–C stretching frequency of the cation ($\nu_2 \approx 1500$ cm^{-1}).

1. Introduction

Acetylene has been the subject of extensive research over recent years not only because it is one of the most abundant species in interstellar space and cometary atmospheres and in various important chemical systems, such as combustion and photolysis of hydrocarbon molecules, but also because its photodynamics in the ultraviolet (UV) and vacuum–UV (VUV) range remains a great challenge to both experimental and theoretical chemists.

The photochemistry of acetylene has been investigated by using resonance lamps [1], ArF excimer lasers at 193 nm [2–5], resonant multiphoton excitation [6] and synchrotron radiation [7–11]. Many studies have been focused on the photoproducts, their internal energy distribution and their subsequent reactions.

In the region below the first ionization limit, different photodissociation processes can occur, leading to the following fragments:

$$C_2H_2 + h\nu \rightarrow C_2H + H \quad (1)$$

$$C_2H_2 + h\nu \rightarrow C_2 + H_2 \quad (2)$$

$$C_2H_2 + h\nu \rightarrow CH + CH \quad (3)$$

* Corresponding author. Fax: +33-1-69156777; e-mail: dolores.gauyacq@ppm.u-psud.fr

0009-2614/99/$ - see front matter
PII: S0009-2614(99)01121-5

The radicals C_2H, C_2 and CH can be produced in their ground state or in electronically excited states when these channels are energetically opened. In addition to dissociation, a non-dissociative relaxation occurs as well, with a significant branching ratio after excitation of acetylene in the same energy range, as was shown by dissociation quantum yield measurements at different wavelengths [12]. Relaxation into triplet vinylidene has been suggested to account for this channel but this hypothesis has not been confirmed by a direct experimental evidence so far.

The previous studies performed at different excitation wavelengths have shown [12] that the dissociation of acetylene is dominated by process (**1**). Although no branching ratio has been measured in the 10 eV excitation region, recent experiments focused on H-fragment detection by Doppler selected time-of-flight (TOF) technique [13,14] and by high-resolution Rydberg H-atom TOF measurements [15] revealed efficient dissociation proceeding also by channel (**1**). In addition, these experiments have provided new information on the internal energy distribution of the C_2H fragment following VUV excitation of some members of the Rydberg super complex 4s + 3d. Polarization studies have also been carried out in these experiments [13–15] and have shown evidence for two competing dissociation mechanisms, one fast (femtosecond timescale), 'direct' mechanism exhibiting polarization dependence, and a slower one (picosecond timescale) leading to a statistical distribution of the fragment internal energy.

The present work is focused on the analysis of the visible fluorescence from photofragments, following photoexcitation of low-pressure acetylene by synchrotron light between 154 and 60 nm. Although similar experiments have been already carried out [9–11], this is the first systematic exploration of the evolution of the fluorescence spectrum from 26 000 cm^{-1} below up to 74 700 cm^{-1} above the IP. Special emphasis has been brought to the excitation of the Rydberg states. In particular, dispersed emission spectra from fragments have been obtained in the same conditions between 350 and 900 nm. Four typical behaviors observed on four specific Rydberg states have been selected for presentation in this Letter.

2. Experimental

The experiment has been performed at the synchrotron radiation facility Super-ACO in Orsay (France). The light beam (SA63) is equipped with a 3-m monochromator with two different gratings (1800 and 2000 grooves/mm), which was tuned for this work in the 154–60 nm region. The photon flux was monitored by measuring the photocurrent emitted from an Au grid, and/or the fluorescence signal from a sodium salicylate deposit receiving the transmitted beam.

Acetylene was introduced into a vacuum chamber by a stainless steel needle with a 100 μm internal diameter at right angle with the VUV beam. A background pressure of about 10^{-4} mbar was maintained in this chamber under operating conditions by two Seiko H1000C and two Leybold TURBOVAC 1000 turbo-molecular pumps. Differential pumping was achieved by means of a VARIAN V70 turbo-molecular pump installed on the tubing between the high-vacuum synchrotron line and the vacuum chamber, supplemented by a series of small diaphragms for the optical path. With this arrangement, it was possible to work without any window up to a pressure of 10^{-3} mbar in the main chamber.

The isotropic visible fluorescence of the fragments was efficiently collected by an original silver-coated ellipsoidal mirror system and coupled into a bundle of silica optical fibers (about 3000 fibers 1.25 m long) guiding the fluorescence signal towards the measurements systems (the optical device for the fluorescence collection will be detailed elsewhere [16]). The advantage of this setup is to permit the measurement of both the transmitted VUV light intensity (and hence to get the absorption data) and the fluorescence signal. The output of the fiber bundle (7×4 mm^2) was coupled either to a photomultiplier tube Hamamatsu R928 (spectral range 950–185 nm) or to the entrance slit of a 0.27 m, f/4, Jobin–Yvon monochromator 270 M (150 grooves/mm grating, 13 nm resolution at 546 nm, spectral range 250–900 nm) equipped with a liquid-nitrogen-cooled CCD matrix detector (256×1024 pixels). With this setup three types of spectrum could be respectively recorded:

- absorption spectra by deriving the absorbance by the classical Beer–Lambert's law $\ln[I(\nu)/I_0(\nu)]$,

where $I_0(\nu)$ represents the transmission curve of the synchrotron beam line monochromator and $I(\nu)$ the transmitted intensity when the sample is present;
- excitation spectra while scanning the beam line monochromator wavelength. In this case, any visible light from 330 to 900 nm was detected whatever the emitting species were; and
- dispersed fluorescence spectra, in the 330–900 nm range, at fixed excitation wavelengths.

After exposures of variable duration (typical accumulation times of 5 min), the CCD image of the whole emission spectrum was averaged over the slit height (256 pixels) and transferred to a computer. Further data treatment was needed in order to remove cosmic rays and instrumental baseline. The data were finally numerically deconvoluted by using the apparatus function (including light detector, monochromator and CCD spectral response), independently determined by scattering white light from the sample position. The dispersed fluorescence spectra shown in Section 3 have been corrected correspondingly.

3. Results and discussion

In the following, we first describe the observed excitation spectra from 154 to 60 nm, which are displayed in Fig. 1, for the low excitation energy range (together with the absorption spectrum), and in Fig. 2, for the high excitation energy range. Then we will discuss the different dissociation pathways observed via the fragment dispersed fluorescence spectra in Fig. 3.

3.1. Total fluorescence spectra below the IP

Fig. 1 shows a panoramic absorption spectrum (bottom panel, b) with the corresponding excitation spectrum (top panel, a) between 153 and 102 nm, with an average instrumental bandwidth of 0.10 nm. Except for a continuum signal arising in the 132 nm region, this spectral region exhibits the prominent s- and d-Rydberg series of acetylene converging to the first ionization potential [17] (the energy position of the $v = 0\,\tilde{X}^2\Pi_u$ ground state of the $C_2H_2^+$ ion is indicated by a dashed line in the figure), as was already observed in a static cell [7]. As shown in the high-resolution absorption spectra analyzed by Herman and Colin [17], most of the observed Rydberg transitions in this spectral region present a more or less diffuse character. The most striking example is given by the lowest member of these series, the $3s\sigma_g\,\tilde{C}^1\Pi_u$ state of which the band origin is lying at 152 nm. This band, as well as the 2_0^1 and 2_0^2 members of the ν_2 progression at 148 and 144 nm, respectively, show a spectral profile much broader than the experimental linewidth, characteristic of a fast relaxation process. This fast process has been recently interpreted by accurate ab initio calculations as a direct and linear dissociation of the $\tilde{C}^1\Pi_u$ state into the $C_2H(\tilde{A}^2\Pi) + H$ products [18]. Due to energy conservation, the excess energy should be distributed into the vibrational levels of the $\tilde{A}$ state of C_2H and should lead to infrared (IR) emission of the ethynyl radical in the region above 1 μm, not observable with the present setup.

The corresponding total visible fluorescence spectrum shown on top of Fig. 1 shows almost no signal between 153 and 136 nm. Then the fluorescence signal gradually increases and, from 123 nm up the 108 nm limit, becomes an almost exact mirror image of the absorption spectrum with the same relative band intensities. As will be shown later, the observed fluorescence in this excitation energy region below the first ionization limit is most essentially due to excited C_2H fragments. In the excitation spectral region of Fig. 1, the $C_2H(\tilde{X})$ and the $C_2H(\tilde{A})$ products are accessible. The $\tilde{A}$–$\tilde{X}$ high-resolution emission spectrum has been studied by several groups [3,19,20] and shows a strong and complex vibronic band structure around 2.7 μm. On the other hand, a visible continuous emission around 500 nm was first reported by Okabe [1] and later by other groups [9,21,22], and was tentatively assigned to emission from an electronically excited doublet state (the '$\tilde{B}$ state') of C_2H, as suggested from earlier ab initio calculations [23]. Recent accurate ab initio calculations have localized the second excited doublet state of the ethynyl radical, namely the $\tilde{B}^2A''$ state at 4.8 eV above the $\tilde{X}^2\Sigma^+$ ground state [24]. Again, energy conservation precludes the production of such $C_2H(\tilde{B})$ fragment above 118 nm. Then, in the low excitation energy region, only vibrationally excited

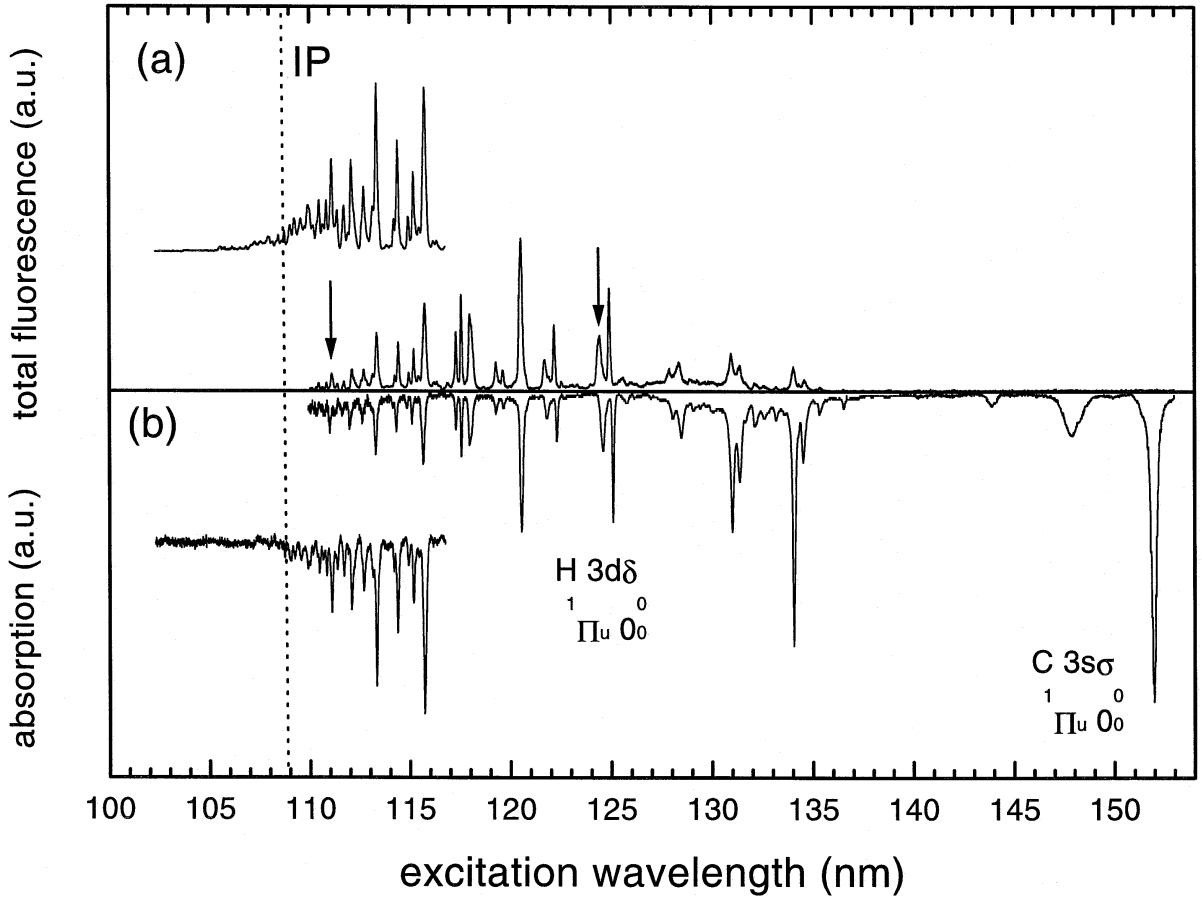

Fig. 1. Fluorescence excitation (a) and absorption (b) spectra of acetylene in the 150–100 nm region, recorded at the synchrotron radiation with a resolution of 0.10 nm. The arrows indicate the excitation wavelengths corresponding to the dispersed fluorescence spectra of Fig. 3.

bands of the $\tilde{A}-\tilde{X}$ system can be proposed as responsible for this visible emission in agreement with the proposition by Bergeat et al. [25]. It is expected that, with increasing excitation energy, higher vibrational levels are populated in the $C_2H(\tilde{A})$ fragment, leading to a visible fluorescence which gradually increases (see Fig. 3 and below).

3.2. Total fluorescence spectra above the IP

Fig. 2 shows the excitation spectrum in the 113–60 nm region. Part of the Rydberg structure below the first ionization potential is also shown in order to be compared with the relative fluorescence intensity above IP. In the spectral region between 105 and 97 nm no fluorescence has been observed. This sharp decrease of the fragment fluorescence at the onset of the ionization channel has been observed in earlier fluorescence studies [7] and it will be discussed below. The broad structure arising between 95 and 70 nm lies below the first excited electronic state of $C_2H_2^+$ and corresponds to excitation of superexcited states as well as overlapping weaker features. These superexcited states have been extensively studied both experimentally and theoretically, [9,10,26–29]. They decay in a substantial fraction to neutral fragments that subsequently emit. The weaker and broad peaks superimposed on these shape resonances have been assigned to Rydberg series converging to the $\tilde{A}\,^2A_g$ state of the ion [9,10], on the basis of earlier theoretical predictions [27–29]. More recently, a precise characterization of the $\tilde{A}\,^2A_g$ state of the ion has

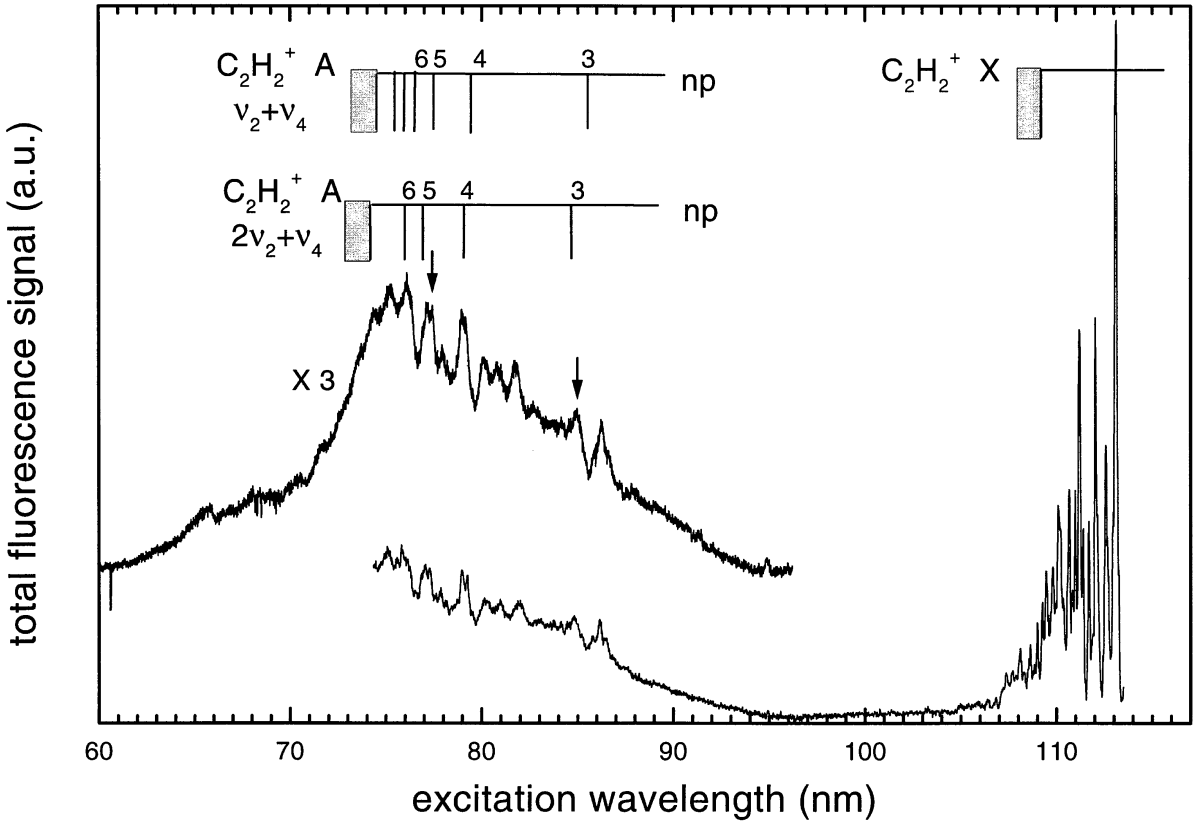

Fig. 2. Total fluorescence excitation spectra of acetylene between the first and second IP. The Rydberg series assignment is discussed in the text. The arrows indicate the excitation wavelengths corresponding to the dispersed fluorescence spectra of Fig. 3.

been determined both theoretically [30] and experimentally [31]. Indeed, this state has been observed by resonantly-enhanced multiphoton-dissociation spectroscopy from the cation ground state. It shows a *trans*-bent equilibrium geometry very different from that of the linear $\tilde{X}\,^2\Pi_u$ ground state. The observed $\tilde{A}$–$\tilde{X}$ transition of the acetylene cation exhibits a very weak 0_0^0 origin band and a strong progression in the ν_4 *trans*-bending mode as well as in the out-of-plane *cis*-bending mode (ν_5) [31], in agreement with the geometry change from the $\tilde{X}$ to $\tilde{A}$ predicted by the calculations [30].

Earlier assignments of these Rydberg series [9,10], were based on linear excited symmetries which is obviously not correct for the series converging to the $\tilde{A}$ state of the ion. Due to the large geometry change from the neutral ground state $\tilde{X}\,^1\Sigma_g^+$ to the $\tilde{A}\,^2A_g$ state of the cation, one expects stronger p series of both a_u and b_u symmetries converging to vibrationally excited levels of the $\tilde{A}\,^2A_g$ state and weaker series converging to the vibrational origin of the $\tilde{A}$ state. Since the largest changes occur in the CC bond length as well as in the CCH angle [30,32], series converging to vibrational levels involving excited ν_2 (CC stretching mode) and ν_4 (*trans*-bending mode) should be observed preferentially. A tentative reassignment is shown in Fig. 2 including two p-Rydberg series with an approximate quantum defect of 0.6 and converging to the $\nu_2+\nu_4$ and $2\nu_2+\nu_4$ levels of the $\tilde{A}$ state. From the ionization potential value of the $\tilde{A}$ state, i.e. 131 115 cm^{-1} [31,33], and from the $\nu_4 = 793$ cm^{-1} value measured by Cha et al. [31], the Rydberg series limits lead to values of around 1500 and 2950 cm^{-1} for ν_2 and for $2\nu_2$, respectively. These values seem reasonable if one compares the geometry of the $\tilde{A}$ state of the ion with that

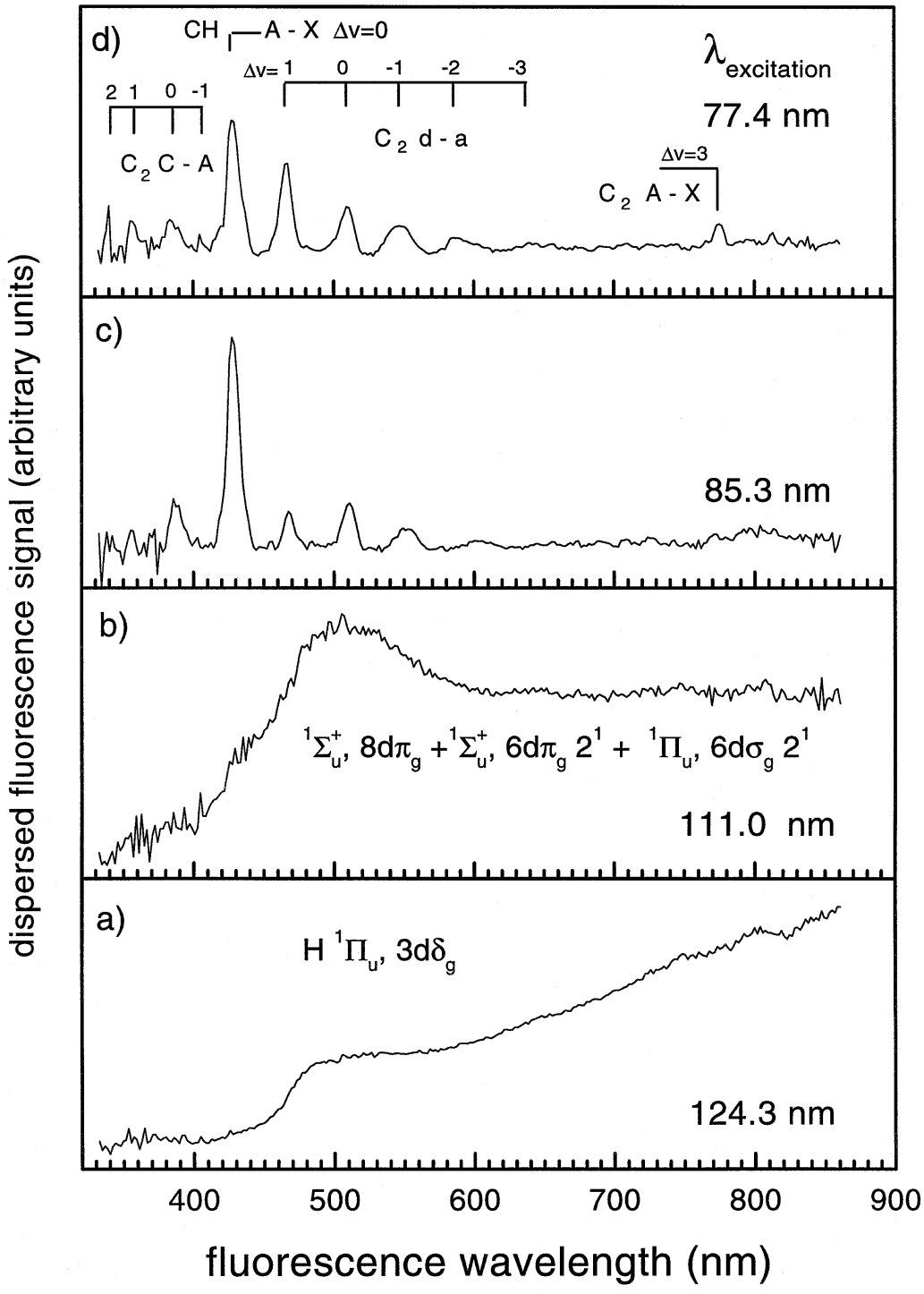

Fig. 3. Dispersed fluorescence of the acetylene photofragments between 330 and 900 nm: (a) excitation of a Rydberg state at 124.3 nm, showing the emission spectrum of C_2H; (b) excitation of Rydberg states at 111.0 nm showing the same emission; (c) excitation at 85.3 nm; (d) excitation at 77.4 nm.

of the $\tilde{A}$ state of the neutral and their respective CC stretch frequencies.

3.3. Dispersed fluorescence spectra and dissociation pathways

Fig. 3 illustrates the nature of the different dissociation pathways of acetylene which can be observed through fragment visible fluorescence at various photoexcitation energies. Four dispersed fluorescence spectra in the range 330–900 nm are shown in this figure. The corresponding excitation wavelengths have been chosen to reach four different Rydberg states which are indicated by arrows on the total fluorescence spectra of Figs. 1 and 2.

3.3.1. Dissociation pathways following Rydberg excitation below the IP

The first two, namely the $3d\delta_g$, $\tilde{H}\,^1\Pi_u$, 0^0 and $8d\pi_g\ ^1\Sigma_u^+$, 0^0 Rydberg states (the later overlapping with the vibrationally excited $6d\pi_g\ ^1\Sigma_u^+$, $2^1 + 6d\sigma_g\ ^1\Pi_u$, 2^1 Rydberg states), converge to the ground state of the ion (panels 3a,b).

These spectra have been normalized to each other with respect to the synchrotron radiation intensity and the absorption line-strengths at 124.3 and 111.0 nm. The continuum emission due to the $\tilde{A}$–$\tilde{X}$ band system of the C_2H fragment (see discussion above and Ref. [25]) is clearly seen in the two spectra. However, they differ significantly, and it should be stressed out that this difference has never been reported in earlier publications (see, e.g., Refs. [9,22]). Spectrum 3a shows a gradual increase of intensity towards long wavelengths, and a small bump around 500 nm. Spectrum 3b is characterized by the prominence of this bump. Such a difference should be associated with a qualitative change in the dissociation mechanism. Indeed, H-fragment spectroscopy of the dissociative $\tilde{H}3d\delta_g\ ^1\Pi_u$ Rydberg state of acetylene has revealed two mechanisms [13–15].

1. A direct one leading to fast H-fragments and low internal energy in the lowest vibrational levels of the $C_2H(\tilde{A})$ fragment which are vibronically mixed with higher vibrational levels of the $C_2H(\tilde{X})$ fragment [19,20]. This mechanism must be responsible for a strong IR emission of C_2H around 2.7 μm. In Fig. 3a, only the rise towards this IR emission is observed.
2. A second mechanism taking place in a longer timescale gives rise to $C_2H(\tilde{A})$ fragments with a significant amount of internal energy. This mechanism has been tentatively explained by Löffler et al. [15] on the basis of a statistical distribution of internal energy over the three vibrational modes of C_2H. This second mechanism must correspond to the continuum emission in the visible part extending down to 450 nm, in the spectrum of Fig. 3a, since it is the only one for which enough internal energy is available in order to radiate in the visible domain.

In our experiment, the two mechanisms cannot be observed separately and they both result in a superposition of both near-IR and visible fluorescence of the fragment.

The observation of emission in the 500 nm range can be understood by considering the potential energy surfaces of the two lowest electronic states of C_2H, calculated by Boggio-Pasqua et al. [24]. Along the stretching coordinates, the two potential energy surfaces remain almost parallel and separated by about 0.5 eV. Along the bending coordinate, the $\tilde{A}\,^2\Pi$ state splits into two Renner–Teller components. The upper $^2A'$ component exhibits an isomerization barrier lying at about 2.5 eV above the ground state at 90° bending angle [34]. As was already proposed by Bergeat et al. [25], emission from the bending levels of the $^2A'$ component lying in the energy region near the top of the barrier toward the ground state should be favored by Franck–Condon factors and would give rise to a quasi-continuum band spectrum with a maximum around 500 nm. Fig. 4 shows a schematic energy diagram in which the energy disposal in the C_2H fragment is mainly distributed among the bending levels of the A state, thus favoring the A–X visible emission. Note that this green emission has not been resolved in any of the earlier works [22], which is consistent with the high level density in this energy range. Then the observed evolution of the dispersed fluorescence spectrum can be qualitatively understood: with increasing total internal energy in the $C_2H(\tilde{A})$ fragment, distribution of level population favors more and more the high bending levels of the

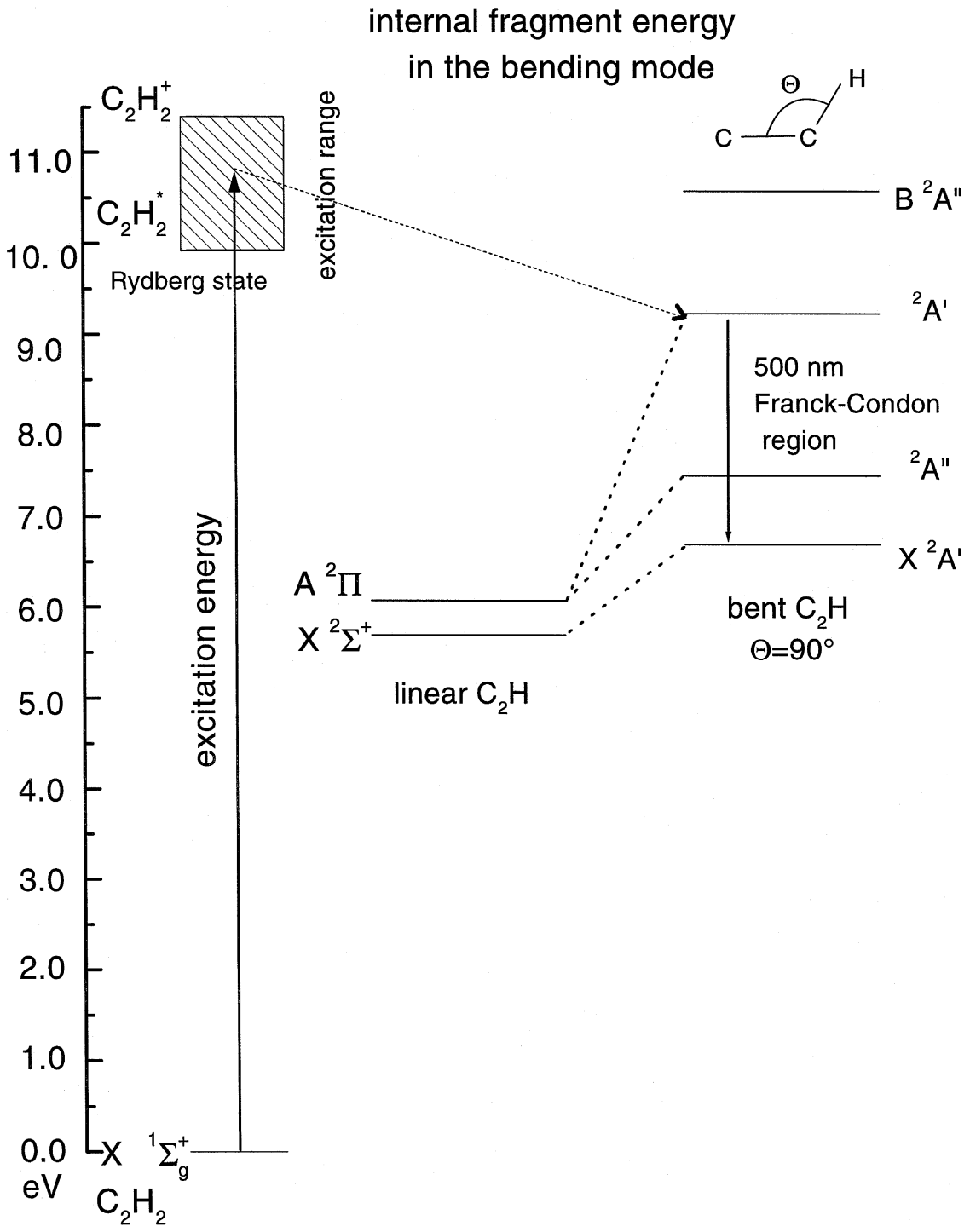

Fig. 4. Schematic energy diagram showing the excitation energy region below the first IP of acetylene and the internal energy of the C_2H fragment along the bending coordinate (see the text).

$\tilde{A}$ state as compared to the lower levels, leading to a more pronounced emission bump around 500 nm in comparison to the IR emission.

Finally, it is remarkable that, at the excitation energy of about 10 eV, corresponding to the fluorescence spectrum of Fig. 3a, most of the internal energy available in the $C_2H(\tilde{A})$ fragment is needed to populate high bending levels of the $\tilde{A}$ state in order to observe a significant emission intensity in the 500 nm region. Therefore, according to the present observation, the bending levels (responsible for the emission near 500 nm) seem to be preferentially populated (as compared to the stretching levels) when the $\tilde{H}$ Rydberg state of acetylene is excited. This is in contradiction with the hypothesis of a statistical distribution proposed in Ref. [15].

3.3.2. Dissociation pathways following excitation above the IP

Fig. 3c,d shows the dispersed fragment emission at the excitation energies, $\lambda = 85.3$ and $\lambda = 77.4$ nm, respectively, of the two upper Rydberg states converging to the first excited state of the ion, as discussed above (see arrows in Fig. 2). These two spectra are also normalized to each other but not to the spectra of Fig. 3a,b. It is remarkable that almost no C_2H continuum remains in these spectra. This absence can probably be related to the sudden drop of the total visible fluorescence (Fig. 2). Such an observation implies that, if excited C_2H is formed by channel (**1**), it should emit in a different spectral region, not accessible with our apparatus. This does not mean that process (**1**) does not occur at higher excitation energies, it just underlines that the internal energy distribution of this fragment is no longer detectable by our visible fluorescence device.

Conversely, new sharp emission bands appear on both figures: the $CH\,A\,^2\Delta–X\,^2\Pi$ $(\Delta v = 0)$ bands, $CH\,B\,^2\Sigma–X\,^2\Pi$ $(\Delta v = 0)$ bands, $C_2\,d\,^3\Pi_g–a\,^3\Pi_u$ $(\Delta v = 1,\ 0,\ -1,\ -2,\ -3)$ Swan bands and C_2-$C\,^1\Pi_g–A\,^1\Pi_u$ $(\Delta v = 2,\ 1,\ 0,\ -1)$ bands, as previously reported [9–11]. In addition to these bands, previously unreported bands from the C_2 Phillips system $(A\,^1\Pi_u–X\,^1\Sigma_g^+)$ with $\Delta v = 3$ (3–0, 4–1 and 5–2) are present in the spectrum of Fig. 3c.

These excited fragments are most probably produced via excitation of the superexcited states populated by the VUV excitation, and to a minor extend via the overlapping Rydberg states. The mechanism for their production seems to follow a direct dissociation pathway, since as shown by Han et al. [9], they all appear just above their thermodynamical thresholds.

Concerning the C_2 fragment, it is still questionable whether it is produced by the sequential dissociation mechanism (**1**) leading to $C_2 + 2H$ or by the concerted process (**2**) leading to $C_2 + H_2$. It has to be noted that in the $CH + CH$ reaction studied by Bergeat et al. [25] the products $C_2 + H_2$ have been observed at a total energy of about 10 eV above the ground state of the acetylene molecule, comparable to the present photon energy. The C_2 production was in this case pressure dependent, and the authors suggested the formation of acetylene molecule followed by a rapid isomerization into vinylidene radical and finally a collision induced dissociation of vinylidene into the $C_2 + H_2$ products. On the basis of the present data on the C_2 fragment production, we cannot distinguish channel (**1**) from channel (**2**). Further studies, including the search of the C_2 apparition threshold, are under progress and should bring more information on this concerted process (**2**).

As a final point, we mention that additional dispersed fluorescence spectra have been recorded by exciting many other Rydberg states below the first IP [35]. They all show the same trend as in Fig. 3a,b. The data analysis is in progress.

4. Summary and conclusion

Visible fluorescence emission of acetylene photofragments under VUV tunable excitation has been observed with an optimized setup adapted by differential pumping to work with unfiltered synchrotron radiation.

The very high sensitivity of the fluorescence collection device as well as a careful deconvolution procedure by the apparatus transmission function have permitted to observe previously unreported features:

1. the evolution of the $\tilde{A}–\tilde{X}$ continuum emission of C_2H with the energy of excited Rydberg states below the first IP has been recorded systematically by exciting a large number of Rydberg

states. The next step will be a theoretical calculation of the fragment emission probability as a function of the excitation energy, in order to explain the evolution of the continuum emission with respect to the red and near-IR emission.

2. a new assignment of the Rydberg series converging to the $\tilde{A}$ state of the acetylene cation is proposed and leads to a reasonable value of the ν_2 frequency of this state taking into account the experimental and theoretical characterization of this state [30,31].

In conclusion, we hope that present and future results will help in the elucidation of the complex photolysis and photochemical processes involved when the acetylene molecule is irradiated by VUV photons.

Acknowledgements

We are grateful to Dr. M. Vervloet for his continuous and efficient help and encouragement during the experimental stage of this work and for his discussions, and Dr. J.C. Loison and Ph. Halvick for interesting and stimulating discussions. We also thank M. Bonneau and S. Bonhomme for their technical assistance. This work has been partially supported by the Programme National 'Physique et Chimie du Milieu Interstellaire' (CNRS, CEA, CNES). Two of us (A.C. and C.F.) acknowledge a Brazilian government (CAPES) visiting grant.

References

[1] H. Okabe, J. Chem. Phys. 62 (1975) 2782.
[2] A.M. Wodke, Y.T. Lee, J. Phys. Chem. 89 (1985) 4744.
[3] T.R. Fletchner, S.R. Leone, J. Chem. Phys. 90 (1989) 871.
[4] J. Segall, Y. Wen, R. Lavi, R. Singer, C. Wittig, J. Phys. Chem. 95 (1991) 8078.
[5] K. Seki, H. Okabe, J. Phys. Chem. 97 (1993) 5284.
[6] Y.-C. Hsu, M.-S. Lin, C.-P. Hsu, J. Chem. Phys. 94 (1991) 7832.
[7] M. Suto, L.C. Lee, J. Chem. Phys. 80 (1984) 4824.
[8] C.Y.R. Wu, T.S. Chien, G.S. Liu, D.L. Judge, J.J. Caldwell, J. Chem. Phys. 91 (1989) 272.
[9] J.C. Han, C. Ye, M. Suto, L.C. Lee, J. Chem. Phys. 90 (1989) 4000.
[10] M. Ukai, K. Kameta, R. Chiba, K. Nagano, N. Kouchi, K. Shinsaka, Y. Hatano, H. Umemoto, Y. Ito, K. Tanaka, J. Chem. Phys. 95 (1991) 4142.
[11] T. Ibuki, Y. Horie, A. Kamiuchi, Y. Morimoto, M.C.K. Tinone, K. Tanaka, K. Honma, J. Chem. Phys. 102 (1995) 5301.
[12] S. Satyapal, R. Bersohn, J. Phys. Chem. 95 (1991) 8004.
[13] L.-H. Lai, D.-C. Che, K. Liu, J. Phys. Chem. 100 (1996) 6376.
[14] J.H. Wang, Y.-T. Hsu, K. Liu, J. Phys. Chem. 101 (1997) 6593.
[15] P. Löffler, E. Wrede, L. Schnieder, J.B. Halpern, W.M. Jackson, K.H. Welge, J. Chem. Phys. 109 (1998) 5231.
[16] S. Douin, A. Campos, S. Boyé, P. Bréchignac, to be published.
[17] M. Herman, R. Colin, Physica Scripta 25 (1982) 275.
[18] J. Lievin, F. Laruelle, private communication.
[19] M. Vervloet, M. Herman, Chem. Phys. Lett. 144 (1988) 48.
[20] P.G. Carrick, A.J. Merer, R.F. Curl Jr., J. Chem. Phys. 78 (1983) 3652.
[21] Y. Saito, T. Hikida, T. Ichimura, Y. Mori, J. Chem. Phys. 80 (1984) 31.
[22] R.K. Sander, J.J. Tiee, C.R. Quick, R.J. Romero, R. Estler, J. Chem. Phys. 89 (1988) 3495.
[23] S.-K. Shih, S.D. Peyerimhoff, R.J. Buenker, J. Mol. Spectrosc. 74 (1979) 124.
[24] M. Boggio-Pasqua, Ph. Halvick, M.-T. Rayez, J.-C. Rayez, J.-M. Robbe, J. Phys. Chem. 102 (1998) 2009.
[25] A. Bergeat, T. Calvo, G. Dorthe, J.-C. Loison, J. Phys. Chem. A 103 (1999) 6360.
[26] R. Uwin, I. Khan, N.V. Richardson, A.M. Bradshaw, L.S. Cederbaum, W. Domcke, Chem. Phys. Lett. 77 (1981) 242.
[27] T. Hayashi, S. Iwata, M. Sasanuma, E. Ishiguro, Y. Morioka, Y. Iidaans, N. Nakamura, J. Phys. B 15 (1982) 79.
[28] P.W. Langhoff, B.V. McKoy, R. Unwin, A.M. Bradshaw, Chem. Phys. Lett. 83 (1981) 270.
[29] L.E. Machado, E.P. Leal, G. Csanak, B.V. McKoy, P.W. Langhoff, J. Elect. Spectrom. Relat. Phenom. 25 (1982) 1.
[30] G. Chambaud, R. Van den Boom, P. Rosmus, Chem. Phys. Lett. 247 (1995) 79.
[31] Ch. Cha, R. Weinkauf, U. Boesl, J. Chem. Phys. 103 (1995) 5224.
[32] G. Herzberg, Molecular Spectra and Molecular Structure, vol. III, Electronic Spectra and Electronic Structure of Polyatomic Molecules, Van Nostrand, New York, 1966.
[33] N. Shafizadeh, J.-H. Fillion, D. Gauyacq, S. Couris, Phil. Trans. Roy. Soc. A 355 (1997) 1637.
[34] Ph. Halvick, private communication.
[35] S. Boyé, A. Campos, S, Couris, Ph. Bréchignac, S. Douin, C. Fellows, N. Shafizadeh, D. Gauyacq, to be published.